



**Unusual Concentration Dependence of the
Photoisomerization Reaction in Donor-Acceptor Stenhouse
Adducts**

Journal:	<i>Photochemical & Photobiological Sciences</i>
Manuscript ID	PP-ART-03-2019-000130.R1
Article Type:	Paper
Date Submitted by the Author:	25-Apr-2019
Complete List of Authors:	Lui, Brandon; University of California at Riverside, Chemistry Tierce, Nathan; University of California at Riverside, Chemistry Tong, Fei; University of California at Riverside, Chemistry Sroda, Miranda ; University of California Santa Barbara, Chemistry and Biochemistry Luo, Hao; Chongqing University Read de Alaniz, Javier; University of California Santa Barbara, Chemistry and Biochemistry Bardeen, Christopher; University of California at Riverside, Chemistry

Unusual Concentration Dependence of the Photoisomerization Reaction in Donor-Acceptor Stenhouse Adducts

Brandon F. Lui⁽¹⁾, Nathan T. Tierce⁽¹⁾, Fei Tong⁽¹⁾, Miranda M. Sroda⁽²⁾, Hao Lu⁽³⁾, Javier Read de Alaniz^{(2)*}, and Christopher J. Bardeen^{(1,3)*}

⁽¹⁾Department of Chemistry
University of California, Riverside
Riverside, CA 92521

⁽²⁾Department of Chemistry and Biochemistry
University of California Santa Barbara
Santa Barbara, CA 93106-9510

⁽³⁾School of Chemistry and Chemical Engineering
Chongqing University
Chongqing 400044, P.R.China

⁽⁴⁾Materials Science and Engineering Program
University of California, Riverside
Riverside, CA 92521

Abstract

Donor-acceptor Stenhouse adducts comprise a new class of reversible photochromic molecules that absorb in the visible and near-infrared spectral regions. Unimolecular photoisomerization reactions are usually assumed to be insensitive to photochrome density, at least up to millimolar concentrations. In this paper, the photoisomerization kinetics of a third-generation donor-acceptor Stenhouse adduct molecule (denoted **DASA**) are examined over a range of concentrations. **DASA** switches efficiently at micromolar concentrations in both liquid solution and in polymers, but as the photochrome concentration is increased there is a dramatic inhibition of the photoisomerization. A kinetic study of both the reactant and photoproduct decays at varying concentrations and in different hosts indicates that the forward photoisomerization and the thermal backward reaction can change by factors of 20 or more depending on **DASA** concentration. Femtosecond transient absorption experiments show that the initial *cis*→*trans* step of the isomerization is not affected by concentration. It is hypothesized that long-range Coulombic interactions interfere with the ground state electrocyclization stage of the isomerization, which is unique to the **DASA** family of photochromes. The physical origin of the

inhibition of photoswitching at high photochrome concentrations must be understood if the **DASA** class of molecules is to be used for applications that require high photochrome concentrations, including photomechanical actuation.

Introduction

The ability of molecules to isomerize after light exposure (photochromism) has enabled applications ranging from data storage to fluorescence microscopy to optical computing. There exist many classes of organic molecules that undergo photoisomerization reactions in dilute liquid solutions, providing a wide array of options for the design of light-responsive materials.^{1,2} Many of these photochromic molecules retain their ability to photoisomerize in solid hosts like polymers. But when photochrome concentrations are increased to the point where intermolecular interactions become non-negligible, the photochemistry can be modulated by the close proximity of the photochromes. Electronic interactions between neighboring molecules can lead to the formation of delocalized excited states (excitons) with different reactivities. Steric interactions can inhibit the nuclear motions necessary to complete the isomerization reaction. In rare cases, molecular interactions can also facilitate the photochemistry, for example through a chain reaction mechanism.³⁻⁵

The effects of high photochrome density on reaction kinetics must be taken into account for some applications. For example, the development of organic photomechanical materials requires high photochrome concentrations because the work density should be directly proportional to the photochrome density.^{6,7} While multiple photochromic molecule classes have exhibited photomechanical behavior in polymer hosts⁸⁻¹¹ and neat crystals¹²⁻²², there is still a need for new and improved photomechanical elements, especially ones that can be activated by visible instead of ultraviolet light.²³ A recently developed class of photochromic molecules

based on donor-acceptor Stenhouse adducts (DASAs) absorb in the visible and near-infrared spectral regions.²⁴⁻³⁰ Even more promising, these molecules are negative photochromes, meaning that the photoproduct absorption shifts to the blue of the reactant absorption and thus does not absorb the exciting light.³¹ This property can lead to high conversion efficiencies due to the avoidance of a photostationary state. The light-driven forward reaction pathway for the CF₃ pyrazolone based DASA derivative (E)-4-((2Z,4E)-2-hydroxy-5-(2-methylindolin-1-yl)penta-2,4-dien-1-ylidene)-2-phenyl-5-(trifluoromethyl)-2,4-dihydro-3H-pyrazol-3-one (referred to as **DASA** in this paper) is shown in Scheme 1.^{32, 33} The reverse reaction is thermally activated and occurs on timescales of seconds to minutes in liquid solution. We became interested in the DASAs as possible active elements for photomechanical materials. Their favorable absorption properties and negative photochromism make them ideal for this application, but highly concentrated samples, or even single crystals, are required in order to generate useful amounts of work.

In this paper, we examine the photochemical properties of **DASA** over a range of concentrations. We focus on the third generation **DASA** molecule shown in Scheme 1 because this derivative has a relatively long-wavelength absorption and good open-form isomer stability.³⁴ We find that **DASA** switches efficiently at low concentrations in both liquid solution and in polymer hosts. As the photochrome concentration is increased, however, the ability of **DASA** to photoswitch decreases drastically. At concentrations on the order of 10⁻³ M, the photoswitching is effectively turned off for moderate light intensities on the order of 1 mW/cm². A similar trend is observed in polymer hosts. A two-state kinetic analysis, combined with photophysical measurements, is used to evaluate how changes in forward and reverse reaction rates conspire to inhibit the net production of the ring-closed isomer. Our results indicate that

the slowdown likely occurs during the proton transfer/ring-closing step, as opposed to the actinic *cis-trans* photoisomerization step. The electrocyclization reaction is unique to the **DASA** family of photochromes and may be vulnerable to environmental effects induced by polar molecules, including neighboring DASAs. The physical origin of the inhibition of photoswitching at high photochrome concentrations must be understood if the **DASA** class of molecules is to be used in photomechanical applications. Such an understanding would provide the basis for designing new **DASA** molecules that can switch efficiently at high concentrations.

Experimental

Sample preparation: The synthesis of **DASA** has been reported previously.³⁴ Chloroform and toluene were purchased from Fischer Chemical. A series of different concentrations ranging from 10^{-6} - 10^{-2} M (chloroform) and 10^{-6} - 10^{-3} M (toluene) were prepared (10^{-2} M was unachievable in toluene due to limited solubility). To make the polymer samples, methylene chloride (Fisher Chemical) was used to prepare a 2.50×10^{-5} M stock solution of **DASA**. Aliquots were taken from this stock to dissolve appropriate amounts of polystyrene and polymethyl(methacrylate), both purchased from Sigma-Aldrich, to create a series of concentrations ranging from 10^{-4} - 10^{-1} M $\left(\frac{mol_{DASA}}{L_{polymer}}\right)$. The films were made by drop casting the **DASA**-polymer solutions on microscope slides purchased from Fisher Scientific. These films were placed in an oven at 80°C to ensure evaporation of residual solvent.

Absorption & transient absorption studies: An Ocean Optics USB4000 was employed to acquire the time-dependent absorption spectra of the samples under irradiation. The OceanView software was used to operate the spectrometer with a wavelength window of 400-800 nm and a

full spectrum with acceptable signal-to-noise could be acquired within 1 s. The neat film and polymer samples were mounted in front of the probe light source and a 638 nm diode laser was used to isomerize the films. For liquid samples, we wanted to ensure that the optical densities were ~ 0.3 or less for reasons discussed below. To achieve this, a demountable flow cell with variable path lengths was employed. (ESI) The 638 nm laser beam was passed through a diffuser to uniformly illuminate the liquid samples with an intensity of 1.0 mW/cm^2 , while a higher intensity of 11.4 mW/cm^2 was used for the polymer samples due to their slower reaction.

Transient absorption measurements were performed using a 1 kHz Coherent Libra femtosecond Ti:Sapphire laser system. The 642 nm pump beam was generated by sending the 800 nm fundamental output into a Palitra optical parametric amplifier. The probe beam was generated by focusing a portion of the fundamental into a 3 mm sapphire plate. Both beams were focused onto either a 0.015 and 0.5 mm path-length quartz flow cell that contained the 1 mM and $30 \mu\text{M}$ DASA/chloroform solutions, respectively. The probe beam after the sample was coupled into an Ultrafast Systems UV-VIS CMOS spectrometer. A solvent response was recorded under the same conditions for all samples in order to remove nonresonant contributions to the transient absorption signal. The transient absorption signals were analyzed using Ultrafast Systems Surface Explorer software.

Differential scanning calorimetry: Glass transition temperatures of the films were collected using a Netzsch 241 Polyma differential scanning calorimeter using a temperature range of 50°C – 150°C with a 20°C heating rate, 1-minute holding, and a 20°C cooling rate. The films were heated and cooled for two cycles and the T_g of the second trial was recorded.

Powder X-ray diffraction (PXRD): A few drops of DASA/toluene solution were deposited onto a clean glass slide (2.5 cm × 2.5 cm) to form a neat film. The glass slide was then put inside an oven at about 90 °C to evaporate the toluene. The PXRD data were collected on a Bruker D8 Advance X-ray powder diffractometer (CuK radiation, $\lambda = 1.5418 \text{ \AA}$, 45 kV/40 mA power) at room temperature. The sample was measured in Bragg-Brentano geometry. The sample holder stage was fixed horizontally and the detector (divergence slit = 0.76 mm without monochromator) rotates over the sample with a step size = 0.0263 degrees.

Results and Discussion

DASA is a polar molecule that is soluble in common organic solvents up to concentrations of ~10 mM. Over the concentration range 10^{-6} - 10^{-2} M in both chloroform (CHCl_3) and toluene, the absorption spectrum remained remarkably constant, as shown in Figure 1. Even at the highest concentrations in these liquids, there is no sign of peak broadening or shifting that would indicate aggregation or electronic coupling. Note that the very high absorption coefficient of **DASA** ($\sim 10^5 \text{ M}^{-1}\text{cm}^{-1}$ at the absorption peak) necessitated the use of variable pathlength demountable cells. At the highest concentrations, the path length had to be reduced to 0.5 micron in order to accurately measure the spectrum and also minimize the variation in light intensity across the cell. This allowed us to assume a constant light intensity within the cell and simplified the kinetic analysis of the photoisomerization rates described below. In all cases the initial sample absorbance at 638 nm was kept at 0.3 or less to ensure that molecules throughout the sample saw a maximum change in light intensity of 50% from front to back of the cell.

When the **DASA** solutions were exposed to 638 nm light, with an intensity of 1.0 mW/cm², the absorption steadily decreased until the forward photochemical reaction rate was balanced by the thermal reverse rate and a photostationary state (PSS) was achieved. An example of this data for CHCl₃ is shown in Figure 2a. In Figure 2b, we plot the time-dependent decrease in the **DASA** absorbance for concentrations ranging from 10⁻⁶ M to 10⁻² M, all under identical irradiation conditions. Both the initial rate of absorbance decay and the asymptotic PSS value change with increasing concentration. A similar concentration dependence was observed in toluene (ESI, Figure S1).

Given that the molecules are free to diffuse and interact in the liquids, we decided to see whether the reaction was also affected by concentration in solid polymer matrices where diffusion is inhibited. The evolution of the **DASA** absorption with concentration is shown for both polymethyl(methacrylate) (PMMA) in Figure 3a and for polystyrene (PS) in Figure 3b. The absorption spectrum of a neat **DASA** film, deposited by solvent evaporation, is also shown in Figure 3b. Only in PS at the highest concentrations (>10⁻² M) are clear signatures of aggregation seen: a broadening of the spectrum and an enhancement of the 0-1 vibronic feature, both of which are probably the result of weakly interacting H-type molecular aggregates.³⁵ In the neat film, the absorption broadened considerably and both blue- and red-shifted features became prominent. The varying peak positions and widths of the spectra in Figure 3 are tabulated in the ESI. Powder x-ray diffraction and polarized light microscopy measurements indicated that the solution-cast neat film was a mixture of crystalline and amorphous regions (ESI, Figure S2). Its absorption lineshape can be understood qualitatively in terms of a statistical mixture of H-type and J-type aggregates.

While there are some differences in the concentration dependence of the absorption spectrum, the polymer blends all showed the same kinetic trends as the liquids: a slowdown in photoswitching as the photochrome concentration is increased. Data for **DASA**/PMMA films are plotted in Figure 4, along with the results for the neat film. As with the liquid samples, the ability of **DASA** to photoisomerize decreases dramatically as the **DASA** concentration increases. Similar results are observed for **DASA** in PS (ESI, Figure S3).

We were curious to see whether another commonly used photochromic molecule would exhibit a similar concentration dependence. We tested the spiroopyran derivative 1,3,3-trimethylindolino-6'-nitrobenzopyrylospiran, which undergoes a ring-opening isomerization to the more polar merocyanine form³⁶, somewhat analogous to the **DASA** isomerization. Over the concentration range 10^{-6} - 10^{-3} M, we found no systematic dependence of either the forward or back reaction rates to within the error, as described in the ESI. Even in neat films, this spiroopyran derivative underwent an obvious color change after a few minutes of exposure to 365 nm light, whereas the **DASA** film showed almost no change for the same photon dose at 638 nm. While this is not a survey of all photochromic molecule classes, it does support that the concentration effect is not a general phenomenon.

In order to quantify the effects of concentration on the **DASA** reaction rates, we can model the isomerization in terms of the simple two-state model given in Figure 5.³⁷ We start with the rate equations

$$\frac{dN_{open}}{dt} = -\sigma I \phi_{OC} N_{open} + k_{back} N_{closed} \quad (1a)$$

$$\frac{dN_{closed}}{dt} = +\sigma I \phi_{OC} N_{open} - k_{back} N_{closed} \quad (1b)$$

where N_{open} and N_{closed} are the concentrations of the open and closed-ring isomers, respectively. $N_{open} + N_{closed} = N_0$ where N_0 is the total chromophore concentration. σ is the absorption cross section of the open form at the irradiation wavelength, ϕ_{OC} is the quantum yield for going from the open to closed form, and k_{back} is the thermal back reaction rate. We assume that before light exposure, all the **DASA** photochromes reside in the open state, $N_{open}(0) = N_0$. While there can be appreciable closed population for some **DASA** derivatives²⁹, at least 95% of the third-generation molecule studied here has been shown to reside in the open form at equilibrium.³⁴ The time-dependence of N_{open} , which is experimentally monitored via its visible absorbance (Abs), is given by:

$$Abs \propto N_{open}(t) = \frac{k_{back}N_0}{k} + N_0 \left(1 - \frac{k_{back}}{k} \right) e^{-kt} \quad (2)$$

where $k = \sigma I \phi_{OC} + k_{back}$ is the initial decay rate of the open-form absorbance. Direct extraction of the initial decay rate k from the curves in Figures 2 and 4 is hampered by the limited acquisition rate of the absorption spectrometer. To measure k_{back} at different concentrations, we monitored the absorption recovery time after the 638 nm irradiation was suddenly removed. In Figure 6a we plot the absorbance recovery for different **DASA** concentrations in toluene, along with fits to the exponential recovery function

$$Abs(t) = Abs(\infty) - Abs(0)e^{-k_{back}t} \quad (3)$$

where $Abs(\infty) - Abs(0)$ is the absorbance right after the 638 nm light is removed and $Abs(\infty)$ is the fully recovered **DASA** absorbance. The curves can all be adequately fit using Equation (3), and we find k_{back} increases by a factor of 7 over this concentration range. In PMMA, we find that the recovery is much slower than in solution (Figure 6b), but again there is a strong

concentration dependence. To determine ϕ_{OC} for the forward reaction, we take advantage of the fact that the ratio of the PSS absorbance to the initial absorbance is given by

$$\frac{N_{open}(\infty)}{N_{open}(0)} = \frac{k_{back}}{k} = \frac{k_{back}}{\sigma I \phi_{OC} + k_{back}} \quad (4)$$

and can be measured with high precision. This ratio, along with the measured values for k_{back} , allowed us to extract values for the forward quantum yield ϕ_{OC} , given a $\sigma(638 \text{ nm})=3 \times 10^{-16} \text{ cm}^2$ (ESI) and a measured intensity of $3.2 \times 10^{15} \text{ photons/s/cm}^2$ ($3.6 \times 10^{16} \text{ photons/s/cm}^2$ in polymer films).

Given the complicated multistep nature of the **DASA** isomerization, the simple two-state model's lack of intermediate states and assumption of negligible open \rightarrow closed isomerization in the absence of light may limit its absolute accuracy. Nevertheless, it does provide a convenient way to quantify **DASA**'s overall photophysical behavior. The concentration dependence of both k_{back} and ϕ_{OC} are plotted in Figure 7a (toluene) and in Figure 7b (PMMA) and the values are summarized in Table 1. In toluene, the forward reaction is inhibited as the quantum yield drops from $\phi_{OC} = 21\%$ for $[\text{DASA}] = 10^{-6} \text{ M}$ to $\phi_{OC} = 3\%$ for $[\text{DASA}] = 10^{-3} \text{ M}$, while k_{back} increases from 0.04 s^{-1} to 0.30 s^{-1} . Both effects inhibit net photoproduct formation. In PMMA, k_{back} is about $100\times$ slower and decreases with increasing **DASA** concentration, the opposite of what is observed in the liquids. Normally, this would favor isomerization, but ϕ_{OC} decreases even more rapidly and again the net effect is to suppress the photochromism at high concentrations. Interestingly, when the rates are plotted versus concentration in a log-log plot (ESI, Figure S4), they exhibit a power law dependence with exponents ranging from 0.3 to 0.7. The origin of this nonlinear behavior with concentration is not clear, and the uncertainties in the log-log plot slopes are sufficiently large we defer further analysis to a future study.

The net quantum yield ϕ_{OC} is actually the product of yields for each reaction step shown in Scheme 1. The question then becomes which stage is responsible for the concentration effect. The first step, *cis*→*trans* isomerization, can be monitored using femtosecond transient absorption spectroscopy. We measured the picosecond dynamics after excitation of the **DASA** at 640 nm for two different concentrations in chloroform, 10^{-5} M and 10^{-3} M. From Table 1, ϕ_{OC} changes by a factor of 2 over this concentration range. A series of time-resolved spectra for different pump-probe delays are shown in Figure 8a. The transient spectra are typical of the **DASA** class of compounds, with a strong excited state absorption feature at 650 nm that decays as isomerization and internal conversion remove population from the excited state.^{38,39} The excited state decay dynamics, measured at the probe wavelength of 648 nm, are overlaid in Figure 8b and are identical. The decay times are the same to within the experimental error, $\tau_{ex} = 25 \pm 2$ ps. After the excited state decay, the derivative lineshape left at longer delays is proportional to the amount of *trans* isomer formed, since its absorption is slightly redshifted relative to that of the *cis* isomer. Since the absorption is not affected by concentration, the size of this feature, relative to the initial bleach, should be proportional to the *cis*→*trans* photoisomerization yield. Here we assume that secondary photon absorption events by the *trans* isomer, which have been shown to facilitate later isomerization events in gas phase experiments³³, are absent in our experiment. This is justified by the fact that the pump pulse is only present during the first 200 fs of the isomerization process and cannot re-excite the *trans* isomer which is formed after several ps. The size of the long-time derivative feature, relative to the initial bleach, is identical for both concentrations (ESI, Figure S5). There is no evidence that the initial *cis*→*trans* reaction step is affected by concentration.

The mechanism for the changes in k_{back} and ϕ_{OC} at high **DASA** concentrations is not clear. We have already ruled out any effects on the *cis*→*trans* step, but it is possible that later steps along the pathway are inhibited. One possible explanation is that steric interference prevents the subsequent conformational change and ring-closing, both of which require substantial atomic rearrangements. But the fact that the inhibition occurs in both liquid and solid-state environments is not consistent with this explanation. Steric inhibition by neighboring **DASA** molecules in a liquid environment is hard to envision. In the solid-state, it is not clear why neighboring **DASA** molecules would be more sterically obstructing than neighboring polymer chains. Such an inhibition has been observed for azobenzene/PMMA blends, but only when the azobenzene begins to crystallize inside the polymer.⁴⁰ Furthermore, if the molecules are close enough to sterically interact with each other, we would expect to see some sign of this association in the absorption spectrum. **DASA**'s large S_0 - S_1 transition dipole moment should lead to excitonic coupling and the appearance of excitonic electronic states. However, changes in the absorption spectrum are only observed at the highest concentrations in PS, while the spectrum in liquids and PMMA do not show changes at any concentration. The absorption data in Figures 1 and 3 show that **DASA** does not form close aggregates at concentrations where there is significant inhibition of the photoisomerization.

We should note that exciton state formation itself can also provide a mechanism for changes in photoreactivity. This mechanism does not require physical contact between the molecule and would be active in both liquid and solid environments. Excitonic coupling has been implicated in lowered photoisomerization quantum yields for aggregated azobenzene⁴¹⁻⁴⁴ and merocyanine photochromes.⁴⁵ This mechanism does not appear to be operative for **DASA**, however. First, as described above, the photoisomerization inhibition is present in samples

where there is no sign of excitonic coupling. Second, at 10^{-3} M, where ϕ_{OC} has decreased by a factor of 10, the average distance between molecules is on the order of 10 nm, much greater than the typical distance over which excitonic interactions occur. Third, excitonic coupling would most likely affect the excited state reactivity, since this is the state that splits and shifts under the influence of the dipole-dipole interaction. As shown above, there is no evidence that the rate of the excited state *cis*→*trans* reaction is perturbed at higher concentrations.

In polymers, it is possible that adding **DASA** changes the host mechanical properties in a way that makes the local environment more resistant to the isomerization. We checked whether **DASA** changes the mechanical properties of the polymer matrix by measuring the glass transition temperature (T_g) of PS as a function of **DASA** concentration. A stiffening of the polymer matrix would be expected to raise the T_g . A T_g value of 105°C was found for neat PS, in good agreement with literature values and the manufacturer's specification.⁴⁶ Adding **DASA** up to concentrations of 10^{-3} M resulted in a slight ($\sim 1^\circ\text{C}$) decrease in T_g (ESI, Figure S6), as usually observed when small molecule additives are mixed with a polymer.⁴⁷ Again, there was no evidence of a physical effect of **DASA** that would make the host less amenable to the conformational changes needed for photoisomerization.

Previous reports of concentration dependent photoisomerization are rare and are sometimes reported without comment on the mechanism.⁴⁸ Excited state quenching by collisions or noncovalent complex formation have been reported^{49, 50} but can be ruled out in this case based on the transient absorption results. Density functional theory calculations estimate a ground state dipole moment on the order of 15 Debye for closely related molecules⁵¹, so it is likely that **DASA** can support long-range electrostatic interactions that can perturb the proton transfer and electrocyclization steps necessary to complete the isomerization. For example, electrostatic

effects due to high ionic strength have been shown to slow down intramolecular proton transfer rates in liquids.⁵² We are currently pursuing this line of reasoning by measuring photoisomerization rates for dilute **DASA** solutions in a variety of solvents, including ionic liquids. More specific intermolecular interactions may also play a role. For example, there are several reports of ground state isomerization reactions that are inhibited by ion-pairing interactions.^{53, 54} Beves and coworkers have recently shown that the colorless closed form of **DASA** can exist as both enolate and diketone forms, and the enolate form is favored at high concentrations.²⁹ They suggest that hydrogen-bonded pairs of cyclic **DASA** molecules can be formed in solution, providing a possible concentration dependent intermediate that could affect the kinetics of forward and backward isomerizations. Finally, it is likely that multiple factors affect the overall photoisomerization yield and recovery. From the data in Figure 7, higher **DASA** concentrations reduce ϕ_{OC} in both liquids and solids. Meanwhile, k_{back} increases in liquids but decreases in the polymers. The different effects in different hosts suggest that the concentration effects depend on the diffusivity of the **DASA** molecules. Additional experiments and theory will probably be needed to sort out the mechanisms responsible for the concentration dependence of the rates.

Conclusion

The results in this paper identify a new effect in the photophysics of **DASA** photochromes: the dramatic inhibition of the photoisomerization with increasing photochrome concentration. Preliminary experiments in our labs indicate that this inhibition is a general effect, observed for different **DASA** derivatives and across a wide variety of solid and liquid hosts. We can eliminate steric and excitonic interactions as possible mechanisms for this

inhibition. Femtosecond transient absorption experiments show that the fast *cis*→*trans* step of the isomerization is not affected by concentration. We suspect that long-range Coulombic interactions interfere with the slower electrocyclization stage of the isomerization. Determining the physical origin of the photoisomerization inhibition at high concentrations is necessary in order to design new **DASA** derivatives that avoid this problem. Many other photochromic molecules (spiropyrans, diarylethenes, azobenzenes) exhibit strong photochromic behavior even in neat crystals or amorphous films, where concentrations are on the order of 1-10 M. DASAs provide an opportunity to expand the molecular toolbox for photomechanical materials if they can maintain their favorable photochromic properties at similar concentrations.

Acknowledgements

This work was supported by the Office of Naval Research through the MURI on Photomechanical Material Systems (ONR N00014-18-1-2624).

Electronic supplementary information (ESI) available: Figures S1–S7 and information on sample preparation, the mathematics of the two-state kinetic model, and tables with additional spectral and kinetic data.

References

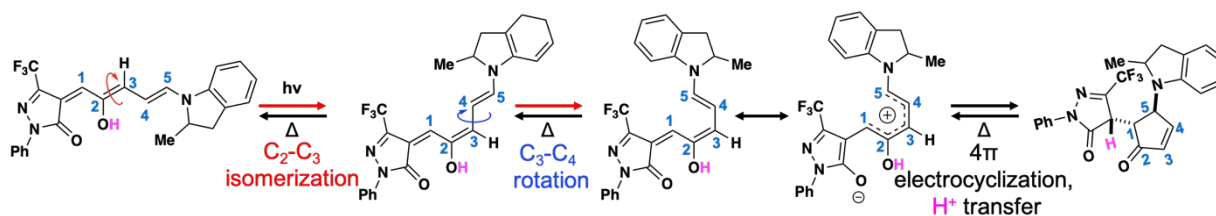
1. H. Durr and H. Bouas-Laurent, *Photochromism : Molecules and Systems*, Elsevier, New York, 1990.
2. M. Irie, Y. Yokoyama and T. Seki, *New Frontiers in Photochromism*, Springer, Japan, 2013.
3. J. Saltiel, D. E. Townsend and A. Sykes, *J. Am. Chem. Soc.*, 1973, **95**, 5968-5973.
4. G. Kuzmanich, M. N. Gard and M. A. Garcia-Garibay, *J. Am. Chem. Soc.*, 2009, **131**, 11606–11614.
5. S. C. Doan, G. Kuzmanich, M. N. Gard, M. A. Garcia-Garibay and B. J. Schwartz, *J. Phys. Chem. Lett.*, 2012, **3**, 81–86.
6. T. Kim, L. Zhu, R. O. Al-Kaysi and C. J. Bardeen, *ChemPhysChem*, 2014, **15**, 400-414.
7. T. J. White, ed., *Photomechanical Materials, Composites, and Systems*, 1 edn., Wiley, Hoboken, New Jersey, 2017.
8. C. J. Barrett, J. Mamiya, K. G. Yager and T. Ikeda, *Soft Matter*, 2007, **3**, 1249-1261.
9. T. Ikeda, J. Mamiya and Y. Yu, *Angew. Chem. Int. Ed.*, 2007, **46**, 506-528.
10. S. Iamsaard, S. J. Abhoff, B. Matt, T. Kudernac, J. J. L. M. Cornelissen, S. P. Fletcher and N. Katsonis, *Nat. Chem.*, 2014, **6**, 229-235.
11. A. H. Gelebart, D. J. Mulder, M. Varga, A. Konya, G. Vantomme, E. W. Meijer, R. L. B. Selinger and D. J. Broer, *Nature*, 2017, **546**, 632-636.
12. R. O. Al-Kaysi, A. M. Muller and C. J. Bardeen, *J. Am. Chem. Soc.*, 2006, **128**, 15938-15939.
13. L. Zhu, F. Tong, N. Zaghoul, O. Baz, C. J. Bardeen and R. O. Al-Kaysi, *J. Mater. Chem. C*, 2016, **4**, 8245-8452.
14. R. Medishetty, A. Husain, Z. Bai, T. Runcevski, R. E. Dinnebier, P. Naumov and J. J. Vittal, *Angew. Chem. Int. Ed.*, 2014, **53**, 5907-5911.
15. P. Naumov, S. Chizhik, M. K. Panda, N. K. Nath and E. Boldyreva, *Chem. Rev.*, 2015, **115**, 12440-12490.
16. O. S. Bushuyev, A. Tomberg, T. Friscic and C. J. Barrett, *J. Am. Chem. Soc.*, 2013, **135**, 12556-12559.
17. H. Koshima, K. Takechi, H. Uchimoto, M. Shiro and D. Hashizume, *Chem. Commun.*, 2011, **47**, 11423-11425.
18. H. Koshima, H. Nakaya, H. Uchimoto and N. Ojima, *Chem. Lett.*, 2012, **41**, 107-109.
19. S. Kobatake, S. Takami, H. Muto, T. Ishikawa and M. Irie, *Nature*, 2007, **446**, 778-781.
20. M. Morimoto and M. Irie, *J. Am. Chem. Soc.*, 2010, **132**, 14172-14178.
21. D. Kitagawa, H. Nishi and S. Kobatake, *Angew. Chem. Int. Ed.*, 2013, **52**, 9320-9322.
22. D. Kitagawa, K. Kawasaki, R. Tanaka and S. Kobatake, *Chem. Mater.*, 2017, **29**, 7524-7529.
23. D. Blegler and S. Hecht, *Angew. Chem. Int. Ed.*, 2015, **54**, 11338-11349.
24. S. Helmy, F. A. Leibfarth, S. Oh, J. E. Poelma, C. J. Hawker and J. R. d. Alaniz, *J. Am. Chem. Soc.*, 2014, **136**, 8169–8172.
25. S. Helmy, S. Oh, F. A. Leibfarth, C. J. Hawker and J. R. d. Alaniz, *J. Org. Chem.*, 2014, **79**, 11316–11329.

26. J. R. Hemmer, S. O. Poelma, N. Treat, Z. A. Page, N. D. Dolinski, Y. J. Diaz, W. Tomlinson, K. D. Clark, J. P. Hooper, C. Hawker and J. R. d. Alaniz, *J. Am. Chem. Soc.*, 2016, **138**, 13960–13966.
27. M. M. Lerch, W. Szymanski and B. L. Feringa, *Chem. Soc. Rev.*, 2018, **47**, 1910-1937.
28. N. Mallo, P. T. Brown, H. Iranmanesh, T. S. C. MacDonald, M. J. Teusner, J. B. Harper, G. E. Ball and J. E. Beves, *Chem. Commun.*, 2016, **52**, 13576-13579.
29. N. Mallo, E. D. Foley, H. Iranmanesh, A. D. W. Kennedy, E. T. Luis, J. Ho, J. B. Harper and J. E. Beves, *Chem. Sci.*, 2018, **9**, 8242-8252.
30. M. M. Lerch, M. Medved, A. Lapini, A. D. Laurent, A. Iagatti, L. Bussotti, W. Szymanski, W. J. Buma, P. Foggi, M. D. Donato and B. L. Feringa, *J. Phys. Chem. A*, 2018, **122**, 955–964.
31. S. Aiken, R. J. L. Edgar, C. D. Gabbutt, B. M. Heron and P. A. Hobson, *Dyes Pigm.*, 2018, **149**, 92-121.
32. M. M. Lerch, S. J. Wezenberg, W. Szymanski and B. L. Feringa, *J. Am. Chem. Soc.*, 2016, **138**, 6344–6347.
33. J. N. Bull, E. Carrascosa, N. Mallo, M. S. Scholz, G. d. Silva, J. E. Beves and E. J. Bieske, *J. Phys. Chem. Lett.*, 2018, **9**, 665–671.
34. J. R. Hemmer, Z. A. Page, K. D. Clark, F. Stricker, N. D. Dolinski, C. J. Hawker and J. R. d. Alaniz, *J. Am. Chem. Soc.*, 2018, **140**, 10425–10429.
35. F. C. Spano, *Acc. Chem. Res.*, 2010, **43**, 429-439.
36. R. Klajn, *Chem. Soc. Rev.*, 2014, **43**, 148-184.
37. K. M. Hanson, S. Narayanan, V. M. Nichols and C. J. Bardeen, *Photochem. Photobio. Sci.*, 2015, **14**, 1607-1616.
38. M. D. Donato, M. M. Lerch, A. Lapini, A. I. D. Laurent, A. Iagatti, L. Bussotti, S. P. Ihrig, M. Medved, D. Jacquemin, W. Szymański, W. J. Buma, P. Foggi and B. L. Feringa, *J. Am. Chem. Soc.*, 2017, **139**, 15596–15599.
39. M. M. Lerch, M. D. Donato, A. D. Laurent, M. Medved, A. Iagatti, L. Bussotti, A. Lapini, W. J. Buma, P. Foggi, W. Szymanski and B. L. Feringa, *Angew. Chem. Int. Ed.*, 2018, **130**, 8195 –8200.
40. C. Pakula, C. Hanisch, V. Zaporojtchenko, T. Strunskus, C. Bornholdt, D. Zargarani, R. Herges and F. Faupel, *J. Mater. Sci.*, 2011, **46**, 2488–2494.
41. C. Gahl, R. Schmidt, D. Brete, E. R. McNellis, W. Freyer, R. Carley, K. Reuter and M. Weinelt, *J. Am. Chem. Soc.*, 2010, **132**, 1831–1838.
42. E. Titov and P. Saalfrank, *J. Phys. Chem. A*, 2016, **120**, 3055–3070.
43. M. Utecht, T. Klamroth and P. Saalfrank, *Phys. Chem. Chem. Phys.*, 2011, **13**, 21608–21614.
44. C. Cocchi, T. Moldt, C. Gahl, M. Weinelt and C. Draxl, *J. Chem. Phys.*, 2016, **145**, 234701/234701-234711.
45. H. Eckhardt, A. Bose and V. A. Krongauzt, *Polymer*, 1987, **28**, 1959-1964.
46. J. Rieger, *J. Therm. Anal.*, 1996, **46**, 965-972.
47. G. t. Brinke, F. E. Karasz and T. S. Ellis, *Macromolecules*, 1983, **16**, 244-249.
48. Y. Nonaka, J. Shimada, H. Nonaka, N. Koike, N. Aoki, Hiroyuki Kobayashi, H. Kase, K. Yamaguchi and F. Suzuki, *J. Med. Chem.*, 1993, **36**, 3731-3733.
49. A. A. Zimmerman, C. M. Orlando, M. H. Gianni and K. Weiss, *J. Org. Chem.*, 1969, **34**, 73-77.
50. A. M. El-Zohry and B. Zietz, *J. Phys. Chem. C*, 2013, **117**, 6544–6553.

51. A. D. Laurent, M. Medved and D. Jacquemin, *Chem. Phys. Chem.*, 2016, **17**, 1846 – 1851.
52. J. F. Joung, S. Kim and S. Park, *Phys. Chem. Chem. Phys.*, 2017, **19**, 25509--25517.
53. G.-A. Craze and I. Watt, *Tet. Lett.*, 1982, **23**, 975-978.
54. A. Yano, Y. Konno, E. Kinoshita and R. Yano, *J. Photochem. Photobiol. A*, 2017, **346**, 411–415.

Toluene			Chloroform		PMMA		
Concentration (M)	k_{back} (s^{-1})	Φ_{OC} (%)	k_{back} (s^{-1})	Φ_{OC} (%)	Concentration (M)	k_{back} (s^{-1}) ($\times 10^{-4}$)	Φ_{OC} (%) ($\times 10^{-3}$)
1×10^{-3}	0.303 ± 0.008	3.3 ± 1.2	0.059 ± 0.001	0.616 ± 0.150	1×10^{-1}	4.4 ± 0.3	7.9 ± 0.9
6×10^{-4}	0.356 ± 0.011	5.4 ± 1.7	--	--	1×10^{-2}	7.6 ± 0.4	15.6 ± 1.4
1×10^{-4}	0.228 ± 0.015	6.7 ± 2.4	0.034 ± 0.001	0.799 ± 0.165	8×10^{-3}	12.5 ± 0.8	39.6 ± 3.5
3×10^{-5}	0.139 ± 0.006	9.5 ± 1.3	0.029 ± 0.001	1.38 ± 0.29	9×10^{-4}	13.5 ± 1.0	209 ± 17
3×10^{-6}	0.046 ± 0.003	21 ± 1.7	--	--			

Table 1. Tabulated quantum yields and recovery rates of **DASA** in toluene, chloroform, and PMMA.



Scheme 1. The photoisomerization of DASA occurs in two steps: 1) an actinic step where a Z→E isomerization along the C₂-C₃ bond occurs, followed by 2) the ground state C₃-C₄ rotation and 4π electrocyclization.

Figures

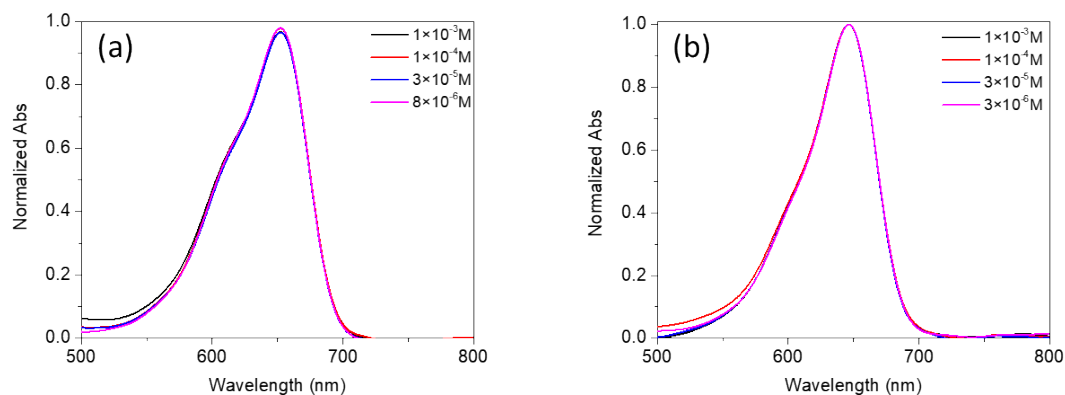


Figure 1. Absorption spectra of DASA at various concentrations. The spectra shape remains unchanged in both (a) toluene and (b) chloroform as the concentration is varied.

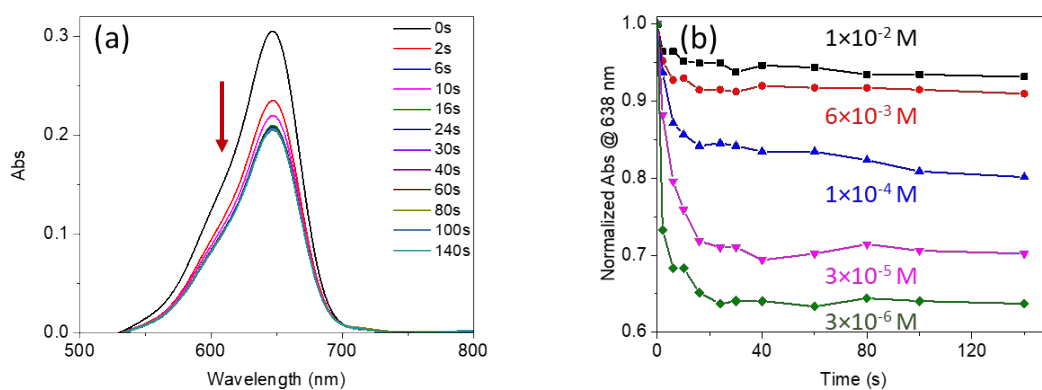


Figure 2. a) DASA absorption spectra at various times for an irradiated $3 \times 10^{-6} \text{ M}$ chloroform sample. A 638 nm laser (0.89 mW/cm^2) irradiated the sample until a photostationary state was obtained. b) The decay of absorption monitored at 638 nm versus time for different DASA concentrations in chloroform.

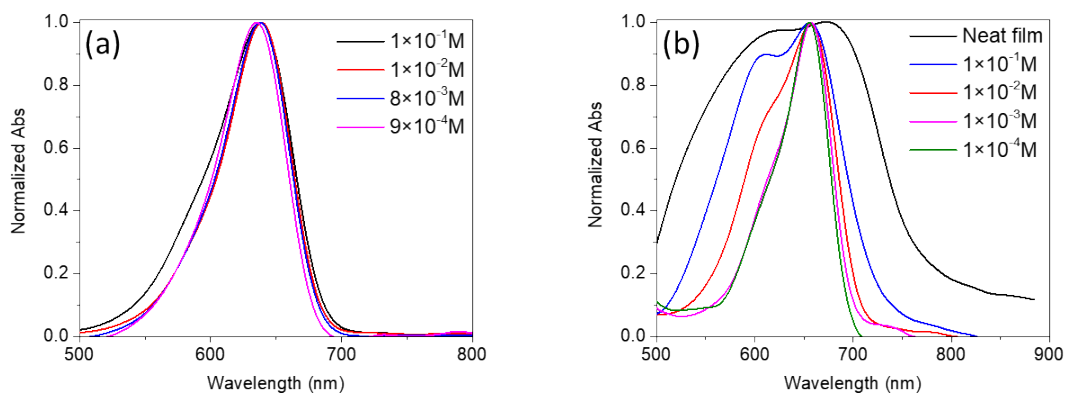


Figure 3. **a)** Normalized absorption spectra of **DASA/PMMA** polymer films with varying **DASA** concentrations. The main peak broadens slightly only at the highest concentration, 0.1 M. **b)** Normalized absorption spectra of **DASA/PS** polymer films with varying **DASA** concentrations. In this polymer, the lineshape broadening starting at 10^{-2} M. Also shown is the absorption of a neat film.

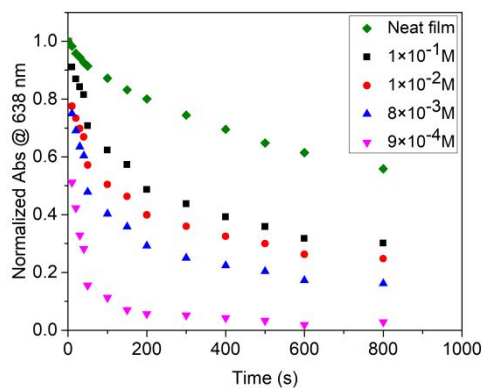


Figure 4. Decay of the **DASA** absorption in PMMA films monitored at 638 nm under irradiation with an intensity of 11.4 mW/cm^2 . The higher intensity was needed to achieve conversion on timescales similar to those in the solutions.

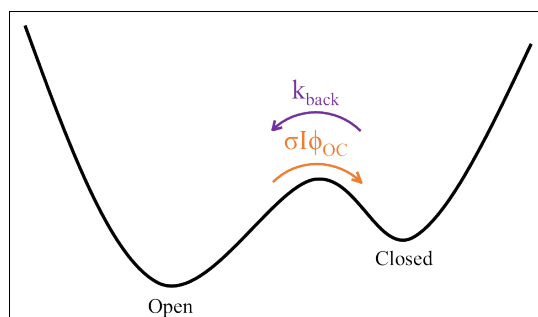


Figure 5. Simple two-state model of the isomerization of **DASA**. The net forward isomerization rate depends on light intensity I , absorption cross section σ , and the net quantum yield for the open \rightarrow closed reaction, ϕ_{OC} . After the light is turned off, **DASA** thermally reverts back to the open form at the rate of k_{back} .

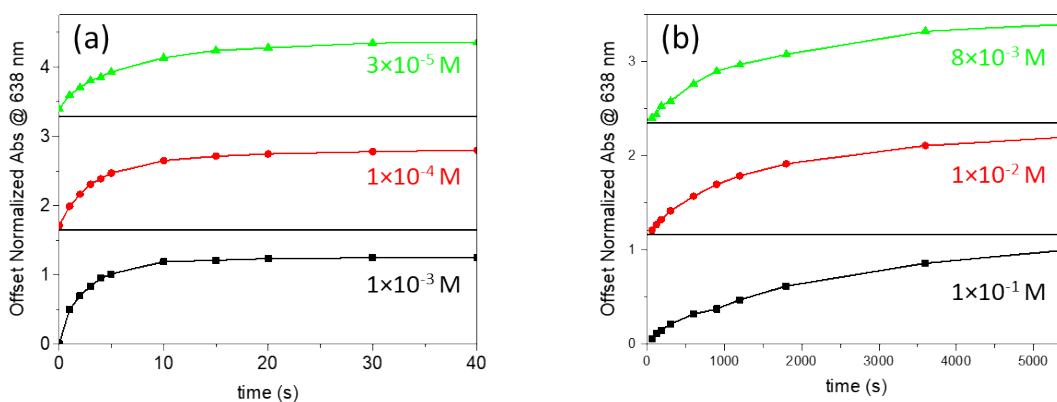


Figure 6. **a)** Absorption recovery curves for different **DASA** concentrations in toluene, monitored at 638 nm, reflecting the decrease in k_{back} . **b)** Absorption recovery curves for different **DASA** concentrations in PMMA, monitored at 638 nm. Unlike the behavior in toluene, k_{back} increases as the **DASA** concentration increases. Exponential fits using Equation (3) to these data allow us to extract the k_{back} values given in Table 1.

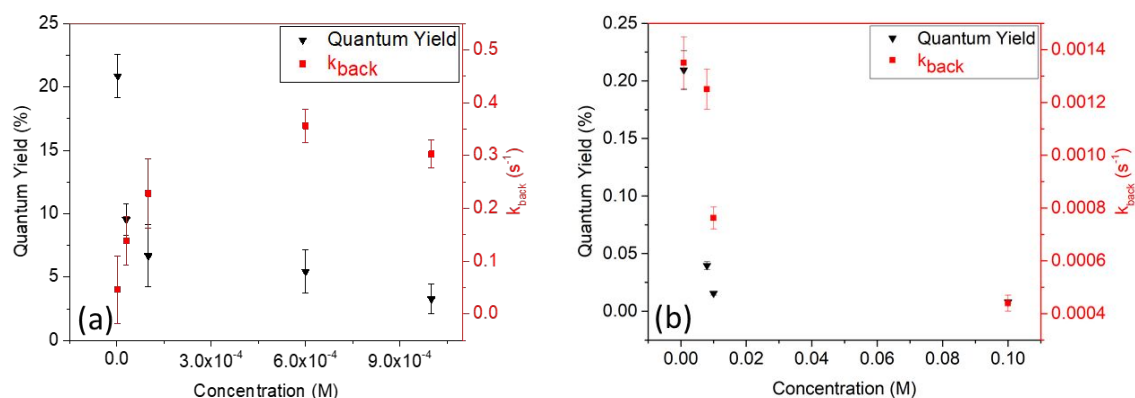


Figure 7. a) The quantum yield (black triangles) and k_{back} rates (red squares) are displayed for **DASA** in toluene for different **DASA** concentrations. In toluene, the QY decreases while k_{back} increases as the **DASA** concentration increases. **b)** The quantum yield (black triangles) and k_{back} rates (red squares) are displayed for **DASA** in PMMA for different **DASA** concentrations. In PMMA, both the QY and k_{back} values decrease as concentration is increased.

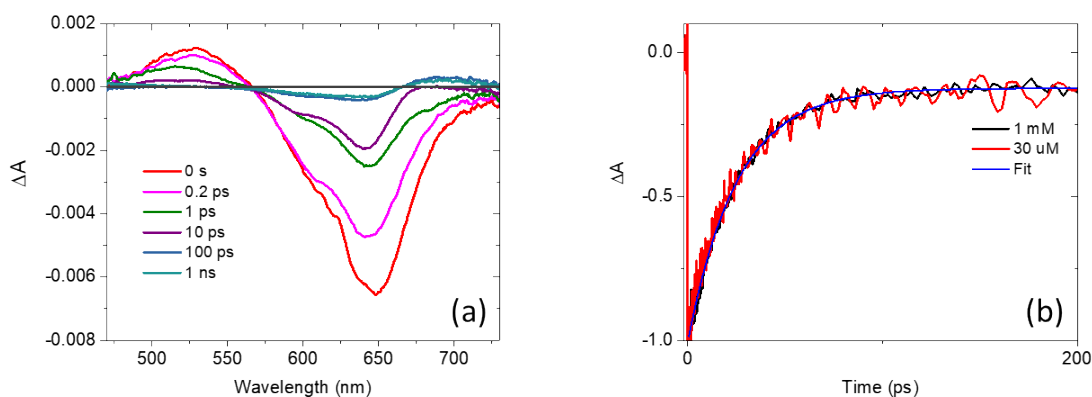
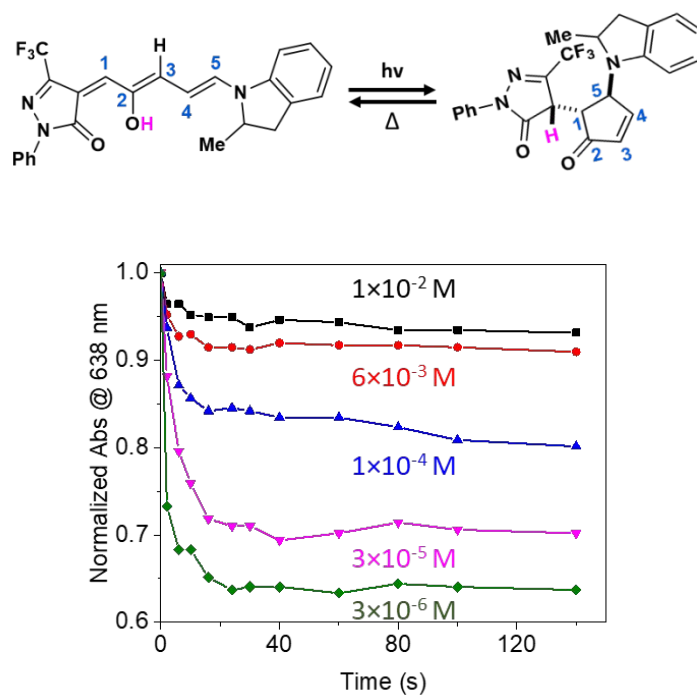


Figure 8. a) Transient absorbance spectra of **DASA** in chloroform (10⁻³ M) for different probe delays. At early times, the positive signal at 528 nm reflects excited state absorbance and the negative signal at 648 nm reflects a ground state bleach and excited state stimulated emission of the *Z* isomer. After 100 ps the excited state features decay to zero, and there is a new positive signal at 695 nm representing the absorbance of the *E* isomer, with a negative bleach signal at around 640 nm. **B)** Normalized decay of the stimulated emission feature at 648 nm shows that the *Z*→*E* isomerization lifetime for the 1 mM and 30 μ M concentrations are identical.



Both forward and backward isomerization reactions of a prototypical donor-acceptor Stenhouse adduct photochrome depend strongly on concentration. The photoisomerization rate decreases with increasing concentration in both liquid and polymer hosts.